CEAS Space Journal (2024) 16:275–283
https://doi.org/10.1007/s12567-023-00495-y

ORIGINAL PAPER

Characterization of polyethylene terephthalate (PET) materials under high-energy electron exposure

Jainisha R. Shah[1] · **Miles T. Bengtson**[2] · **Sydney Collman**[1] · **Ryan C. Hoffmann**[3] · **Dale C. Ferguson**[3] · **Daniel P. Engelhart**[4] · **Elena A. Plis**[1,5]

Received: 17 October 2022 / Revised: 31 March 2023 / Accepted: 3 April 2023 / Published online: 12 April 2023

Abstract

External spacecraft materials play an important role in satellite protection from the harsh space environment.Research has shown that the physical, chemical, and optical properties of matter change continuously as a result of exposure to solar radiation and aggressive chemical species produced in Earth's upper atmosphere. Thorough knowledge of the material properties evolution throughout a planned mission lifetime helps to improve the reliability of spacecraft. Moreover, the establishment of correlation factors between true space exposure and accelerated space weather experiments at ground facilities enables accurate prediction of on-orbit material performance based on laboratory-based testing. The presented work evaluates the radiation effects of different doses of high-energy electron exposure on surface morphology, optical, and charge transport properties of two materials from the PET family, Melinex®454 and Mylar®M021.

Keywords High-energy electron exposure · Geosynchronous Earth orbit (GEO) · Low Earth orbit (LEO) · Reflectance spectroscopy · Surface morphology · Charge transport

1 Introduction

Polyethylene terephthalate (PET) materials are proposed for many applications in a spacecraft industry, including construction of inflatable structures for satellite de-orbiting, [1] deployable membrane antenna structures [2], fabrication of flexible and stretchable electronics for harsh radiation environment [3, 4], and foldable organic solar cell arrays manufacturing [5, 6]. Most importantly, PET films are utilized in multilayer insulation (MLI) blankets that are employed on the exterior surfaces of spacecraft for passive thermal control purposes. Spacecraft operate in a harsh and demanding environment, which requires materials that can withstand extreme conditions such as temperature fluctuations, high levels of radiation, and vacuum. The ability to maintain an acceptable temperature range during all phases

Jainisha R. Shah and Elena A. Plis have contributed equally to this work.

✉ Jainisha R. Shah
shah@assurtech.com

Miles T. Bengtson
AFRL.RVBorgmailbox@us.af.mil

Sydney Collman
collman@assurtech.com

Ryan C. Hoffmann
AFRL.RVBorgmailbox@us.af.mil

Dale C. Ferguson
AFRL.RVBorgmailbox@us.af.mil

Daniel P. Engelhart
dpengelhart@unm.edu

Elena A. Plis
Elena.Plis@gtri.gatech.edu

1 Assurance Technology Corporation, 84 South Street, Carlisle, MA 01741, USA

2 Postdoctoral Fellow, National Research Council Research Associateship Program, Kirtland AFB, Albuquerque, NM 87117, USA

3 Air Force Research Laboratory, Space Vehicles Directorate, Kritland AFB, Albuquerque, NM 87117, USA

4 Department of Chemistry and Chemical Biology, University of New Mexico, 1128 University Blvd NE, Albuquerque, NM 87102, USA

5 Georgia Tech Research Institute (GTRI), 925 Dalney St NW, Atlanta, Georgia 30318, USA

of operation is an important task to ensure the success of the mission [7, 8].

MLI composite materials work by limiting the amount of radiative heat transfer through multiple layers of thin reflectors (shields) and spacer materials. The shields are generally PET or polyimide (PI) metal-coated films with high mechanical strength and low thermal conductivity. An ideal thermal blanket completely reflects the incident radiation. Although these perfect reflectance characteristics have not been obtainable in practice yet [9] and research is being conducted on alternatives to traditional MLI blankets, such as those based on silica aerogels [10–13], which offer improved reflectivity and durability, PET-based shields are still an essential part of spacecraft thermal control system.

By nature of their usage, MLI blankets are exposed to harsh space weather environments comprising high vacuum, solar ultraviolet (UV) radiation, thermal cycling, and impacts from micrometeoroids and artificial orbital debris. At low Earth orbit (LEO), single-oxygen atoms (atomic oxygen, AO) are the prevailing source of material degradation whereas at geosynchronous Earth orbit (GEO), highly energetic electrons are the dominant species interacting with the spacecraft surface [14, 15].

Space-weather events can cause damage to the MLI layers on spacecraft. This damage can weaken the adhesive that holds the layers of MLI together, leading to their delamination [16, 17] thus contributing to the population of high-area-to mass (HAMR) space debris objects in orbit [18]. By comparing the reflectance spectra of the HAMR objects with the laboratory spectra of known spacecraft materials, researchers were able to identify the specific reflective material present in the MLI layers. This finding supports the hypothesis that the HAMR debris was formed as a result of delamination of the MLI layers [19–22].

The effects of dominant GEO environment species, high energy electrons, on mechanical and charge accumulation properties of PI [23] and PET [24–28] films causing the degradation and fragmentation of MLI have been studied. However, the number of studies devoted to the optical changes of PET under the influence of space weather are limited [29] even though understanding these optical changes is invaluable for identifying and tracking debris clouds and determining the origin of space debris [30–32]. This task is accomplished by comparing the reflectance spectra of observed orbital bodies (such as HAMR objects) with a library of known (laboratory) reflectance spectra of different materials. However, if PET layers are changing under the influence of space weather, this must be taken into account when analyzing and interpreting reflectance spectra. Any changes in the optical properties of PET could potentially lead to incorrect identification of debris materials. Moreover, the radiation-induced alteration of optical properties may serve as a proxy measurement for other, less tractable measurements such as electrical conductivity, embrittlement, surface morphology, and chemical reactivity.

In the presented work we studied changes of surface morphology, optical, and charge transport properties of two materials from the PET family, Melinex®454 and Mylar®M021, under high-energy (100 keV) electron irradiation. Evaluation of space weather effects on the change in material properties of MLI components is helpful for understanding of on-orbit characteristics of external spacecraft materials. Various techniques were employed to access the radiation-induced materials dynamics, such as atomic force microscopy (AFM), directional hemisperical reflectance (DHR), and surface potential decay (SPD) measurements. Additionally, we present the astronomical color index of chosen materials as a function of electron fluence.

The astronomical color index of a given material is a convenient metric that is experimentally tractable to remote observers in situations where measurement of a full reflection spectrum is not feasible [33]. A body of literature is available on the utilization of the filter photometry approach for optical observation data analysis and interpretation. For example, Payne et al [34] emphasized the importance of color indices to distinguish the satellites with different configurations. Further, Cowardin et al [35] used the same approach to determine the man-made space body fragment brightness distribution. Beamer et al [36] used the color-color technique for analyzing the wavelength band intensity of reflected light from objects in space. Pearce et al [37] used the clustering of the color indices of Russian SL-12 rocket bodies for the identification of one unique object (SL-12 RB 2012-012D). Finally, attempts to classify spacecraft materials into families according to color index derived from their reflectivity spectral curves were reported by Reyes et al [31]. In our recent work [30] we compared all possible color indexes combinations of g' (406–544 nm), r' (558–682 nm), i' (705–835 nm), and the z' (838–1094 nm) passbands of Sloan Digital Sky Survey (SDSS) [38] astronomical filter set to illustrate the importance of the proper choice of filter combinations since the use of some filter combinations result in more dramatic radiation-induced changes to the color index of the material. Knowledge of the evolution of a material' color index may be harnessed to provide information about a material' chemical state and physical properties using remote observations [35–37, 39].

2 Experimental Details

2.1 Materials

This study was conducted using two PET materials, 5 mil (127 μm) thick Melinex®454 film and 9 mil (229 μm) thick

Mylar®M021 film from DuPont de Nemours, Inc. Visually, the pristine Melinex®454 sample appears as a high clarity film with both sides pre-treated to promote adhesion to most Industrial coatings. Pristine Mylar®M021 is a low shrinkage, low moisture absorption, and high thermal durability film with a white opaque appearance. The studied materials had no coatings applied.

2.2 Irradiation Procedure

Samples were irradiated with high energy (100keV) mono-energetic electron radiation from a Kimball Physics EG8105-UD flood electron gun in the Spacecraft Charging and Instrument Calibration Laboratory (SCICL) at Kirtland Air Force Base in New Mexico, USA [40]. The energy of the electron beam was selected based on the continuous slowing down approximation (CSDA) ranges of high-energy electrons [41]. The details regarding the anticipated estimate of penetration depth of 100 keV electrons into each material is not investigated and surpass the scope of this manuscript. It is important to recognize that the space environment is characterized by a broad distribution of electron energies, which can cause energy deposition and charging of spacecraft surfaces.

Samples were mounted over a carousel that rotated through the hot spot of the electron beam to ensure uniform irradiation. Sample size was 2.5 cm^2 and reflective metal surface of the same area was utilized as a backing substrate.Copper tape and aluminum foil were employed as backing materials for both irradiation experiments, respectively. Prior to electron bombardment, a dehydration bake-out of the loaded carousel was performed for 12 h at 60^0 C using a vacuum oven. More details of the electron irradiation procedure have been reported elsewhere [42]. Irradiation was performed with two different electron beam fluences, 8.5 x 10^{13} electrons/cm^2 and 9.2 x 10^{14} electrons/cm^2, corresponding to 6 h and 24 h of irradiation time, respectively, which could be representative of a range of different space environments. During materials irradiation, background pressure was 3×10^{-7} Torr. The temperature of the sample holder was not measured.

2.3 Characterization Methods

2.3.1 Optical properties

The directional hemispherical reflectance (DHR) of PET samples was measured *in situ* before and during the electron irradiation process in accordance with the optical data acquisition procedure reported elsewhere [43]. In particular, the data collection procedure began by measuring white and black standards (Spectralon and Acktar Black, respectively) using a Spectralon integrating sphere mounted on a robotic arm. The Spectralon sphere was then moved to measure each of the samples mounted on the rotating platform. During the 10-minute measurement process, the electron beam was extinguished to avoid doing damage to the Spectralon standard.

In addition, the optical properties of pristine and radiation-damaged samples were assessed in the UV/Vis (200–800 nm) spectral region using a Cary 2000 spectrophotometer with spectral resolution of 2 nm. Finally, color ratio plots were generated using astronomical Sloan Digital Sky Survey (SDSS) [38] filters to show changes in spectral brightness as a function of electron fluence [31]. Color ratio plots were generated from the measured reflectance curves calculating the ratio of brightness between two filter passbands (color index) using the equation 1

$$A - B = -2.5\left(\frac{I_A}{I_B}\right) \tag{1}$$

where A and B represent the two filter passbands of interest, and I_x is the brightness of the band x obtained by integrating the reflectance curve over the wavelength range of a given band. Differences between the brightness in the g’ band (408–545 nm) and the z’ band (865–960 nm) were determined.

2.3.2 Surface characterization

Surface morphology and roughness of studied materials were examined using Bruker Dimension ICON atomic force microscopy (AFM) allowing measurement of surface roughness up to 5 μm on areas as large as 200 μm x 200 μm.

2.3.3 Charge transport properties

The volume resistivity of pristine and irradiated PET samples was evaluated using the surface potential discharge (SPD) measurements [44] performed in a vacuum environment with a low-energy (5 keV) Kimball Physics EGPS-2017B electron gun and a TREK probe model 370 high-speed electrostatic voltmeter. The back surface of the sample was attached to the grounded backplane via copper tape with conductive adhesive. To conduct the SPD experiment, the front surface of the irradiated material was bombarded by a beam of electrons during a short period of time, 1-2 s, immediately after which the non-contact voltmeter was positioned 1-2 mm from the surface and began to record the surface potential. After the front of the charge body had reached the grounded backplane, the dissipation of charge was primarily determined by the loss of electrons from the material. SPD measurements were performed in darkness to eliminate the possibility of optically excited states obscuring our analysis. Using the SPD method, the dark resistivity of the material may be derived from a plot of surface potential versus time, or decay curve, using equation 2:

$$\rho = \frac{\tau}{\epsilon_0 \epsilon_r} \tag{2}$$

where τ is charge decay time in seconds determined from the linear fit of the post-transit region of the decay curve. It represents the time it takes electrons deposited from the beam to traverse the material and be lost to the grounded backing plate. The ϵ_0 and ϵ_r are the permittivity of free space and relative permittivity of the material, respectively. The conductivity of the material is then calculated as inversely proportional to the resistivity of the material. Whereas the constant voltage method conforming to ASTM D-257 standard is commonly utilized by the material manufacturers to attest the charge transport properties, the SPD method is more applicable to test materials with irradiation-induced heterogeneity under space-simulated conditions [45].

2.4 Sample handling

Unlike radiation-induced material degradation measured by the *in situ* DHR measurements which were performed under high vacuum conditions (< 10^{-6} Torr), the post-irradiation measurements such as AFM or UV/Vis optical tests were performed at different facilities, necessitating considerable air exposure to the materials between their irradiation and characterization. Since air has been shown to obfuscate results for electron irradiated organic polymers (e.g., [46]), handling and characterization protocols of the irradiated air-sensitive materials must be scrutinized and carefully controlled. To reduce the healing rate of PET materials irradiated with high energy electrons upon exposure to atmosphere, the two-stage sample packaging procedure comprising vacuum sealing performed with a Henkelman® industrial vacuum sealer was employed [47].

3 Results

Figure 1 shows representative AFM scans for each studied sample under different electron irradiation dose. Table 1 summarizes the measured surface roughness values of pristine and electron-irradiated samples. Average surface roughness (R_a) values were the average of several 5μm x 5μm scans taken at different parts of the respective samples.

Surface roughness of both PET materials decreased after LEO irradiation with 8.5 x 10^{13} electrons/cm^2 fluence which is attributed to the coalescence of some of the original defects. Higher irradiation fluence, 9.2 x 10^{14} electrons/cm^2, caused the formation of multiple point defects, probably arcing sites, which contribute to the increased average roughness of the materials. The surface between the arcing sites is smoother compared to the pristine material and this is easier to observe for the Mylar®M021.

Absolute hemispherical reflectance of Mylar®M021 and Melinex®454 samples measured at zero electron fluence of impinging 100 keV electrons (pristine material), and two

Table 1 Surface roughness of pristine and electron-irradiated polymer samples

Fluence (e/cm^2)	Mylar®M021, R_a (nm)	Melinex®454, R_a (nm)
Pristine	7.8	8.2
8.5 x 10^{13}	3.6	5.0
9.2 x 10^{14}	4.2	7.6

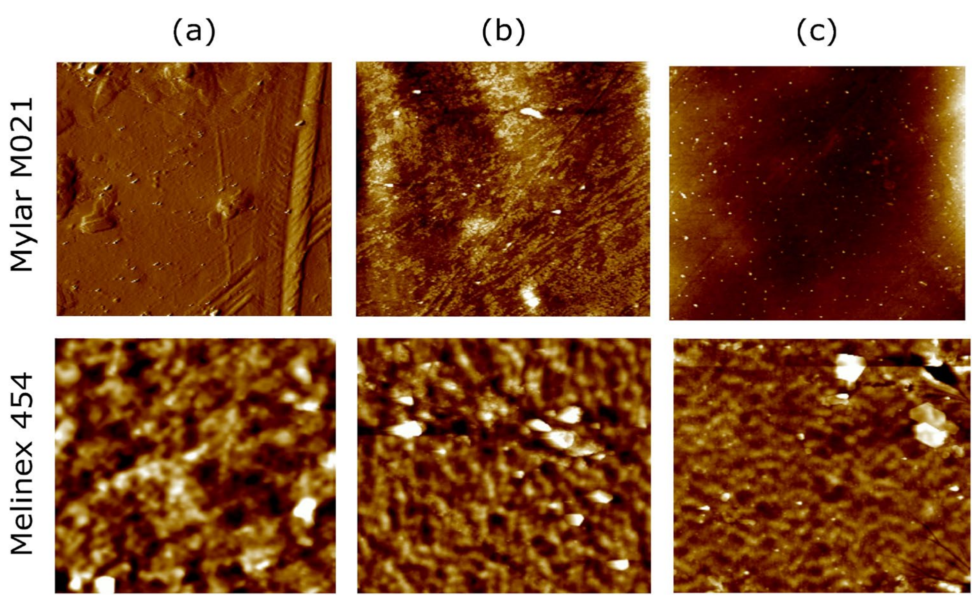

Fig. 1 Representative 5μm x 5μm AFM scans of (a) pristine and electron-irradiated with (b) 8.5 x 10^{13} electrons/cm^2 and (c) 9.2 x 10^{14} electrons/cm^2 PET materials

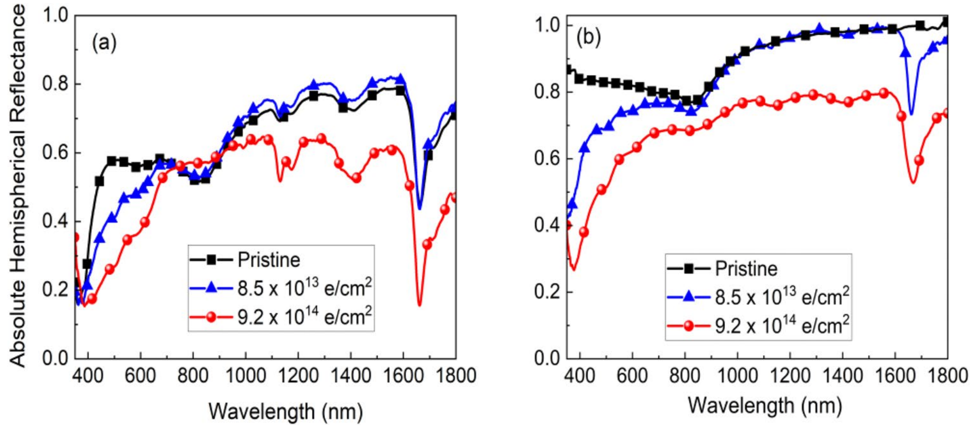

Fig. 2 Absolute hemispherical reflectance curves for (a) Mylar®M021 and (b) Melinex®454 samples irradiated with different fluences of 100 keV electrons measured during irradiation

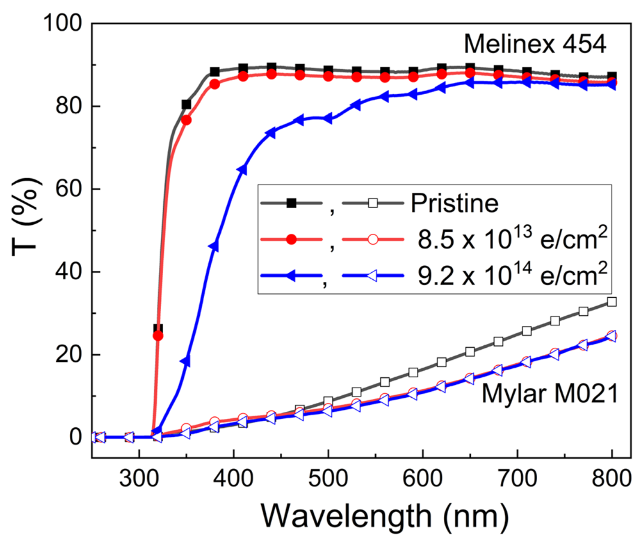

Fig. 3 UV–Vis transmittance spectra of Mylar®M021 and Melinex®454 samples irradiated with different fluences of 100 keV electrons

Table 2 Volume resistivity of Mylar®M021 and Melinex®454 samples

		ρ ($\Omega \cdot$ cm)
Mylar®M021	Pristine	4.3 x 10^{18}
	8.5 x 10^{13}	4.8 x 10^{21}
	9.2 x 10^{14}	3.8 x 10^{19}
Melinex®454	Pristine	9.6 x 10^{18}
	8.5 x 10^{13}	7.5 x 10^{18}
	9.2 x 10^{14}	1.6 x 10^{19}

different electron fluences is shown in Fig. 2. The aluminum backing of the materials served as an optical mirror during the DHR measurements, making the "reflection spectra" superpositions of reflected and transmitted light.

The UV–Vis transmittance spectra of Mylar®M021 and Melinex®454 samples that were exposed to different fluences of 100 keV electrons are shown in Fig. 3. Transmittance of both irradiated samples is decreased with an increase of irradiation dose, more for Melinex®454 than for the Mylar®M021.

The volume resistivity values of Mylar®M021 and Melinex®454 samples irradiated with different fluences of 100 keV electrons measured by SPD method are summarized in Table 2.

The astronomical color index of a given material is a convenient metric that is experimentally tractable to remote observers in situations where measurement of a full reflection spectrum is not feasible [33]. Among twelve possible combinations of the g', r',i', and z' filters from the SDSS astronomical filter set, the g'-z' color index showed the greatest variation as a function of electron fluence and this filter combination was applied to the investigated films [30].

4 Discussion

Whereas the shape of the absolute hemispherical reflectance spectrum of Mylar®M021 film is more complicated than that of the Melinex®454, several common features are identified, such as the absorption band at 830 nm which is attributed to the partial light absorption in the aluminum of the backing plate. Intensity of the 1650 nm feature is not significantly affected by electron irradiation, indicating that whatever chemical moiety is responsible for it is not influenced by the impinging high energy electrons.

A notable decrease of absolute reflectance of both materials in a short wavelength range, 400–675 nm for Mylar®M021 and 400–830 nm for Melinex®454, was observed with increased exposure duration to the high energy electrons. Further increase in electron irradiation dose caused the 20% decrease in reflectance values in 830–1800 nm range of Melinex®454 film. Oppositely, the Mylar®M021 film showed a nearly constant value of absolute hemispherical reflectance in 1000–1800 nm region, with a maximum of 10% reflectance increase in 830–1000 nm range. The latter may be due to the radiation-promoted smoothness due to the radiation-induced crosslinking of the Mylar®M021 compared to the pristine material, since the reduced roughness causes a decrease of the spreading of reflected light and, consequently, promotes more specular light. Although there is a lack of available data on the relationship between the reflected light and the radiation-changed topography of PET materials, researchers have investigated the impact of surface roughness on reflected light intensity in other materials such as pigmented plastics and paper [48, 49].

The decreased transmittance of the electron-irradiated PETs suggests that exposure to high-energy electrons leads to a decrease in the optical transparency of these films. This decrease in transmittance can be attributed to the formation of defects and color centers in the films due to the ionization and excitation of the polymer chains by the high-energy electrons.

The radiation stability of PET has been observed by other researchers [50] and was attributed to the modification of aromatic rings from di-substituted to mono-substituted benzene groups [22]. The condensation of aromatic rings into compact carbonaceous clusters may also result in increased absorption of PET materials in a short wavelength range. Indeed, the increased absorption of the irradiated PET films, beyond 500 nm for Mylar®M021 and in 300–600 nm range for Melinex®454, is shown in Fig. 2.

Interestingly, the volume resistivity of the electron-irradiated PET samples either increased (Mylar®M021) or did not change significantly (Melinex®454). The similar phenomenon has been observed by Chaudhary et al [51] and Oproiu et al [52] (decreased conductivity of PET after electron irradiation) and is attributed to the increased crosslinking of the PET chains due to the electron irradiation, which may obstruct the charge carrier hopping from one chain to another chain resulting in decrease of electrical conductivity. This result is surprising, considering that one successful method for increasing the conductivity of other organic polymers based on a polyimide backbone (such as Kapton®) is to introduce conductive carbon clusters into the polymer. Studies of the role of crosslinking in surface roughening of electron-irradiated PET films are limited; however, the smoother surface of electron-irradiated PET samples may also be a manifestation of radiation-induced increased cross-linking and demonstrates an example of another aromatic thermoplastic, polystyrene [53]. One very promising technique to study the fundamental causes of these changes is in-situ vibrational spectroscopy, a technique that is currently in development in the SCICL lab in collaboration with the University of New Mexico.

The g'-z' color index plot was utilized for the characterization of spectral brightness with increased electron fluence of both studied PET materials. As shown in Fig. 4, both materials demonstrated a monotonic increase of g'-z' versus electron fluence characteristics, resulted in a change of the g'-z' index by factor of 6.3 from the initial (pristine) to the irradiated with maximum electron fluence values for both samples, in particular, from of 0.08 to 0.50 for Mylar®M021 and from 0.15 to 0.95 for Melinex®454. By understanding these optical changes i.e. the spectral regions over which the materials are stable and those where it varies with electron exposure, remote observers can get information about the material's state. This knowledge about the history of the material would be invaluable for identifying and tracking debris clouds and determining the origin of the space debris

5 Conclusion

By understanding the behavior of satellite components throughout their mission lifetime, Earth-based observers may glean more detailed information from unresolved imagery to help prevent space-based catastrophes and to better understand the on-orbit life cycle of commonly used spacecraft materials. This knowledge of on-orbit material degradation will inform spacecraft designers and enable the construction of more robust spacecraft designs as well as improve the abilities of spacecraft operators to conduct accurate and timely anomaly resolution.

In this paper, we investigate a dependence between changes in optical behavior and other material properties of two PET polymers irradiated with high-energy electrons.

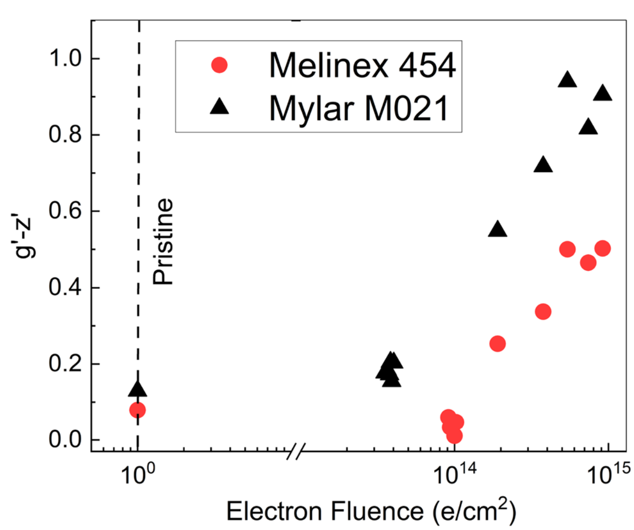

Fig. 4 g'-z' color index of pristine and irradiated with different fluences of 100 keV electrons Mylar®M021 and Melinex®454 samples

The alteration of volume conductivity observed in both types of PET materials following electron irradiation, which could be indicative of diverse space environments, implies that differential spacecraft charging models, such as NASA/Air Force Spacecraft Charging Analyzer Program (NASCAP), should be revised to incorporate time- and environment-dependent material properties to accurately account for material aging. Further, as these polymers are among commonly used spacecraft surface materials, the accompanying optical changes may be of a magnitude that is discernible via resolved or unresolved remote imaging

Acknowledgements Authors would like to thank DuPont de Nemours, Inc, for providing materials for this research.

Author Contributions JRS and EAP conceptualized the idea of the study. JRS, SC, and MTB performed all the experiments reported in this manuscript excluding the surface morphology and FTIR measurements which were performed by EAP. Optical, charge transport, and surface morphology data were analysed by JRS, DPE, and EAP. Manuscript was written by JRS and EAP. RCH, DPE, and DCF reviewed, provided feedback, and approved the manuscript.

Funding This work was partially supported by Air Force Office of Scientific Research, Remote Sensing and Imaging Physics Portfolio (Dr. Michael Yakes) Grant 20RVCOR024 and Georgia Tech Research Institute Independent Research and Development (IRAD) program.

Data availability Not applicable

Code Availability Not applicable

Declarations

Disclaimer The views expressed are those of the author and do not necessarily reflect the official policy or position of the Department of the Air Force, the Department of Defense, or the U.S. government.

Conflict of interest Authors declare no conflict of interest/competing interests.

Ethical approval Not applicable

Consent to participate All authors consented to the participation in research described in this manuscript.

Consent for publication All authors consented to the publication of this manuscript.

References

1. Koryanov, V., Toporkov, A., Kazakovtsev, V., Nedogarok, A.: The technology of using inflatable structures made of special materials to adapt the de-orbiting system for removing spacecraft. In: IOP Conference Series: Materials Science and Engineering, vol. 812, p. 012006 (2020). IOP Publishing
2. Liu, Z.-Q., Qiu, H., Li, X., Yang, S.-L.: Review of large spacecraft deployable membrane antenna structures. Chin J Mech Eng **30**(6), 1447–1459 (2017)
3. Almuslem, A.S., Shaikh, S.F., Hussain, M.M.: Flexible and stretchable electronics for harsh-environmental applications. Adv Mater Tech **4**(9), 1900145 (2019)
4. Cordill, M.J., Taylor, A.A., Berger, J., Schmidegg, K., Dehm, G.: Robust mechanical performance of chromium-coated polyethylene terephthalate over a broad range of conditions. Philoso Mag **92**(25–27), 3346–3362 (2012)
5. Zhao, X., Hao, H., Dong, J., Cheng, F., Hao, J., Xing, J., Liu, H.: Fast extraction of electron across the interface of nanowire ch3nh3pbi3/zno on flexible pet substrate. Materials Letters **197**, 139–142 (2017)
6. Liu, C., Xiao, C., Xie, C., Li, W.: Flexible organic solar cells: Materials, large-area fabrication techniques and potential applications. Nano Energy **89**, 106399 (2021)
7. Meseguer, J., Perez-Grande, I.: Spacecraft thermal control woodhead publishing limited (2012)
8. Gilmore, D.G., Gilmore, D.G., Donabedian, M.: Spacecraft Thermal Control Handbook vol. 1. Aerospace Press El Segundo, CA, ??? (2002)
9. Cepeda-Rizo, J., Gayle, J., Ravich, J.: The multilayer insulation (MLI) blanket. In: Thermal and Structural Electronic Packaging Analysis for Space and Extreme Environments, pp. 33–40. CRC Press, ??? (2021)
10. Hasan, M.A., Rashmi, S., Esther, A., Bhavanisankar, P.Y., Sherikar, B.N., Sridhara, N., Dey, A.: Evaluations of silica aerogel-based flexible blanket as passive thermal control element for spacecraft applications. J Mater Eng Perform **27**(3), 1265–1273 (2018)
11. Petroffe, G., Beouch, L., Cantin, S., Chevrot, C., Aubert, P.-H., Dudon, J.-P., Vidal, F.: Thermal regulation of satellites using adaptive polymeric materials. Solar Energy Mat Solar Cells **200**, 110035 (2019)
12. Nikpourian, H., Bahramian, A.R.: Thermo-physical properties of multilayer super insulation: The role of aerogel blanket. Thermal Sci Eng Progress **20**, 100751 (2020)
13. Fesmire, J.E.: Aerogel-based insulation materials for cryogenic applications. In: IOP Conference Series: Materials Science and Engineering, vol. 502, p. 012188. IOP Publishing (2019)
14. Pilipenko, V., Yagova, N., Romanova, N., Allen, J.: Statistical relationships between satellite anomalies at geostationary orbit and high-energy particles. Adv Space Res **37**(6), 1192–1205 (2006)
15. Han, J.-H., Kim, C.-G.: Low earth orbit space environment simulation and its effects on graphite/epoxy composites. Composite structures **72**(2), 218–226 (2006)
16. Flegel, S.K., Gelhaus, J., Möckel, M., Wiedemann, C., Krag, H., Klinkrad, H., Vörsmann, P.: Multi-layer insulation model for master-2009. Acta Astronautica **69**(11–12), 911–922 (2011)
17. Krag, H., Klinkrad, H., Jehn, R., Flegel, S., Schildknecht, T.: Conclusions from esa space debris telescope observations on space debris environment modelling. In: Proceedings of the European Conference on Space Debris, Darmstadt, Germany (2009)
18. Früh, C., Kelecy, T.M., Jah, M.K.: Coupled orbit-attitude dynamics of high area-to-mass ratio (hamr) objects: influence of solar radiation pressure, earth's shadow and the visibility in light curves. Celestial Mechanics Dynamical Astronomy **117**(4), 385–404 (2013)
19. Cowardin, H., Abercromby, K., Barker, E., Seitzer, P., Mulrooney, M., Schildknecht, T.: An assessment of geo orbital debris photometric properties derived from laboratory-based measurements. In: Advanced Maui Optical and Space Surveillance Technologies Conference, 1, 25 (2009)
20. Barker, E., Abercromby, K.J., Abell, P.: Reflectance spectra comparison of orbital debris, intact spacecraft, and intact rocket

bodies in the geo regime. In: 5th European Conference on Space Debris (2009)
21. Schildknecht, T., Vananti, A., Krag, H., Erd, C.: Physical characterization of high amr debris by optical reflectance spectrometry. In: Proceedings of the International Astronautical Congress, p. 6 (2010)
22. Steckenreiter, T., Balanzat, E., Fuess, H., Trautmann, C.: Chemical modifications of pet induced by swift heavy ions. Nuclear Instruments Methods Phy Res Sect B: Beam Interactions with Mater Atoms **131**(1–4), 159–166 (1997)
23. Plis, E.A., Engelhart, D.P., Cooper, R., Johnston, W.R., Ferguson, D., Hoffmann, R.: Review of radiation-induced effects in polyimide. App Sci **9**(10), 1999 (2019)
24. Czeremuszkin, G., Latreche, M., Wertheimer, M.: Charging/discharge events in coated spacecraft polymers during electron beam irradiation in a scanning electron microscope. Nuclear Instrument Methods Phy Res Sect B: Beam Interact with Mater Atoms **185**(1–4), 88–99 (2001)
25. Hoffmann, R., Cooper, R., Engelhart, D., Plis, E., Ferguson, D.: Localized electron trap modification as a result of space weather exposure in highly disordered insulating materials. Technical report, AIR FORCE RESEARCH LAB KIRTLAND AFB NM KIRTLAND AFB (2017)
26. Griseri, V.: Behavior of dielectrics in a charging space environment and related anomalies in flight. IEEE Transa Dielect Electrical Insulation **16**(3), 689–695 (2009)
27. Edwards, D.L., Hubbs, W.S., Wertz, G.E., Hoppe, D.T., Nehls, M.K., Hollerman, W.A., Gray, P.A., Semmel, C.L.: Electron radiation effects on candidate solar sail material. High Perform Polymers **16**(2), 277–288 (2004)
28. Kupchishin, A.I., Taipova, B.G., Voronova, N.A., Kupchishin, A.A., Shakhanov, K.: Dose dependences of the mechanical strength of polymer materials. In: Key Engineering Materials, vol. 781, pp. 25–29. Trans Tech Publ (2018)
29. Engelhart, D.P., Murray, V.J., Plis, E.A., Fulford, K., Ferguson, D.C., Hoffmann, R.: Effect of electron flux on the degradation of organic polymers in a simulated geo environment. In: AIAA Scitech 2021 Forum, p. 0066 (2021)
30. Engelhart, D.P., Reyes, J.A., Murray, V.G., Ferguson, D.C., Hoffmann, R.C.: Identifying radiation induced spectroscopic changes in polyimide materials. The Journal of the Astronautical Sciences, 1–11 (2022)
31. Reyes, J.A., Cowardin, H.M.: Spectral characterization of spacecraft materials used in hypervelocity impact testing. In: Algorithms, Technologies, and Applications for Multispectral and Hyperspectral Imaging XXVII, vol. 11727, p. 117271 (2021). International Society for Optics and Photonics
32. Reddy, V., Battle, A., Campbell, T., Chodas, P., Conrad, A., Engelhart, D., Frith, J., Furfaro, R., Farnocchia, D., Hoffmann, R., et al.: Spectral characterization of 2020 so (2021)
33. Payne, T.E., Castro, P.J., Moody, J.W., Beecher, E.A., Fisher, M.D., Acosta, R.I.: A discrimination analysis of sloan and johnson photometric systems for non-resolved object characterization. In: Advanced Maui Optical and Space Surveillance Technologies Conference (AMOS) Conference Proceedings (2016)
34. Payne, T.E., Gregory, S.A., Dentamaro, A., Ernst, M., Hollon, J., Kruchten, A., Chaudhary, A.B., Dao, P.D.: Development and evaluation of new methods for estimating albedo-areas for three-axis stabilized geosynchronous satellites. J Astro Sci **66**, 170–191 (2019)
35. Cowardin, H., Seitzer, P., Abercromby, K., Barker, E., Buckalew, B., Cardona, T., Krisko, P., Lederer, S.: Observations of titan iiic transtage fragmentation debris. In: Advanced Maui Optical and Space Surveillance Technologies (AMOS) Conference (2013)
36. Beamer, D., Abeywickrema, U., Banerjee, P.: Polarization vector signatures for target identification. In: Polarization Science and Remote Sensing VIII, vol. 10407, p. 104070. International Society for Optics and Photonics (2017)
37. Pearce, E.C., Ford, H.A., Schildknecht, T., Reddy, V., Block, A.D., Rockowitz, K.: Rapid characterization of geosynchronous space debris with 5-color near-ir photometry. In: Proceedings AMOS Conference (2017)
38. Kent, S.M.: Sloan digital sky survey. Astrophysics and Space Science **217**(1), 27–30 (1994)
39. Reyes, J.A.: Reflectance spectral characterization and taxonomy applications of spacecraft materials to aid space situational awareness (2022)
40. Cooper, R., Hoffman, R.: Jumbo space environment simulation and spacecraft charging chamber characterization. Technical report, Air Force Research Laboratory, Space Vehicles Directorate Kirtland AFB (2015)
41. Pal, P., Varshney, V., Gupta, D.: Approximate expressions for continuous slowing down approximation ranges of high energy electrons and positrons. Nuclear Instruments Method Phy Res Sect B: Beam Interactions with Materials Atoms **21**(1–4), 14–19 (1987)
42. Engelhart, D.P., Plis, E., Humagain, S., Greenbaum, S., Ferguson, D., Cooper, R., Hoffmann, R.: Chemical and electrical dynamics of polyimide film damaged by electron radiation. IEEE Transact Plasma Sci **45**(9), 2573–2577 (2017)
43. Bengtson, M., Maxwell, J., Hoffmann, R., Cooper, R., Schieffer, S., Ferguson, D., Johnston, W.R., Cowardin, H., Plis, E., Engelhart, D.: Optical characterization of commonly used thermal control paints in a simulated geo environment. In: The Advanced Maui Optical and Space Surveillance Technologies Conference, p. 33 (2018)
44. Frederickson, A.R., Dennison, J.R.: Measurement of conductivity and charge storage in insulators related to spacecraft charging. IEEE transact nuclear sci **50**(6), 2284–2291 (2003)
45. Plis, E.A., Engelhart, D.P., Likar, J., Hoffmann, R.C., Cooper, R., Ferguson, D.: Electrical behavior of carbon-loaded kapton for spacecraft applications. J Spacecraft Rockets **55**(3), 775–777 (2018)
46. Plis, E.A., Engelhart, D.P., Cooper, R., Ferguson, D.C., Hoffmann, R.: Effect of environment on charge transport properties of polyimide films damaged by high-energy electron radiation. J Vacuum Science Tech B, Nanotech Microelect: Materials, Proces, Measurement, Phenomena **36**(5), 052906 (2018)
47. Collman, S., Plis, E.A., Shah, J.R., Bengtson, M.T., Hoffmann, R.C., Ferguson, D.C.: Operational procedure for handling of spacecraft materials sensitive to atmospheric exposure. Journal of Spacecraft and Rockets, 1–4 (2022)
48. Arino, I., Kleist, U., Rigdahl, M.: Effect of gloss and texture on the color of injection-molded pigmented plastics. Polymer Eng Sci **45**(5), 733–744 (2005)
49. Xu, R., Fleming, P.D., Pekarovicova, A., Bliznyuk, V.: The effect of ink jet paper roughness on print gloss. J Imag Science Technol **49**(6), 660–666 (2005)
50. Mishra, R., Tripathy, S., Sinha, D., Dwivedi, K., Ghosh, S., Khathing, D., Müller, M., Fink, D., Chung, W.: Optical and electrical properties of some electron and proton irradiated polymers. Nuclear Instruments and Methods in Physics Research Section B: Beam Interactions with Materials and Atoms **168**(1), 59–64 (2000)
51. Chaudhary, N., Koiry, S., Singh, A., Tillu, A., Jha, P., Samanta, S., Debnath, A., Aswal, D., Mondal, R., Acharya, S.: Electron beam induced modifications in flexible biaxially oriented polyethylene terephthalate sheets: Improved mechanical and electrical properties. Materials Chem Phy **189**, 237–244 (2017)
52. Oproiu, C., Martin, D., Toma, M., Marghitu, S., Jianu, A.: Transitory and permanent effects of electron beam irradiation on insulating materials. Nuclear Instruments and Methods in Physics

Research Section B: Beam Interactions with Materials and Atoms **166**, 669–675 (2000)
53. Ting, Y.-H., Liu, C.-C., Park, S.-M., Jiang, H., Nealey, P.F., Wendt, A.E.: Surface roughening of polystyrene and poly (methyl methacrylate) in Ar/O_2 plasma etching. Polymers **2**(4), 649–663 (2010)